Interstitial Zn Atoms Do the Trick

Atomic surfaces defined by the zero flux condition of the different atoms in the Zn_4Sb_3 structure viewed nearly along the *c* axis. For more information see the following pages.

 DOI: 10.1002/chem.200400327

Interstitial Zn Atoms Do the Trick in Thermoelectric Zinc Antimonide, Zn_4Sb_3: A Combined Maximum Entropy Method X-ray Electron Density and Ab Initio Electronic Structure Study

Fausto Cargnoni,[e] Eiji Nishibori,[b] Philippe Rabiller,[c] Luca Bertini,[e] G. Jeffrey Snyder,[d] Mogens Christensen,[a] Carlo Gatti,*[e] and Bo Brummerstadt Iversen*[a]

Abstract: The experimental electron density of the high-performance thermoelectric material Zn_4Sb_3 has been determined by maximum entropy (MEM) analysis of short-wavelength synchrotron powder diffraction data. These data are found to be more accurate than conventional single-crystal data due to the reduction of common systematic errors, such as absorption, extinction and anomalous scattering. Analysis of the MEM electron density directly reveals interstitial Zn atoms and a partially occupied main Zn site. Two types of Sb atoms are observed: a free spherical ion (Sb^{3-}) and Sb_2^{4-} dimers. Analysis of the MEM electron density also reveals possible Sb disorder along the *c* axis. The disorder, defects and vacancies are all features that contribute to the drastic reduction of the thermal conductivity of the material. Topological analysis of the thermally smeared MEM density has been carried out. Starting with the X-ray structure ab initio computational methods have been used to deconvolute structural information from the space-time data averaging inherent to the XRD experiment. The analysis reveals how interstitial Zn atoms and vacancies affect the electronic structure and transport properties of β-Zn_4Sb_3. The structure consists of an ideal $A_{12}Sb_{10}$ framework in which point defects are distributed. We propose that the material is a 0.184:0.420:0.396 mixture of $A_{12}Sb_{10}$, $A_{11}BCSb_{10}$ and $A_{10}BCDSb_{10}$ cells, in which A, B, C and D are the four Zn sites in the X-ray structure. Given the similar density of states (DOS) of the $A_{12}Sb_{10}$, $A_{11}BCSb_{10}$ and $A_{10}BCDSb_{10}$ cells, one may electronically model the defective stoichiometry of the real system either by n-doping the 12-Zn atom cell or by p-doping the two 13-Zn atom cells. This leads to similar calculated Seebeck coefficients for the $A_{12}Sb_{10}$, $A_{11}BCSb_{10}$ and $A_{10}BCDSb_{10}$ cells (115.0, 123.0 and 110.3 $\mu V K^{-1}$ at $T = 670$ K). The model system is therefore a p-doped semiconductor as found experimentally. The effect is dramatic if these cells are doped differently with respect to the experimental electron count. Thus, 0.33 extra electrons supplied to either kind of cell would increase the Seebeck coefficient to about 260 $\mu V K^{-1}$. Additional electrons would also lower σ, so the resulting effect on the thermoelectric figure of merit of Zn_4Sb_3 challenges further experimental work.

Keywords: ab initio calculations · antimony · electron density topology · electronic structure · maximum entropy method · thermoelectric materials · zinc

[a] M. Christensen, Prof. B. B. Iversen
Department of Chemistry, University of Aarhus
8000 Aarhus C (Denmark)
Fax: (+45) 8619-6199
E-mail: bo@chem.au.dk

[b] Dr. E. Nishibori
Department of Applied Physics, Nagoya University
Furo-cho, Chikusa, Nagoya 464-8603 (Japan)

[c] Dr. P. Rabiller
Université de Rennes 1, UMR CNRS 6626
35042 Rennes (France)

[d] Dr. G. J. Snyder
Jet Propulsion Laboratory, 4800 Oak Grove Drive
Pasadena, CA 91109 (USA)

[e] Dr. F. Cargnoni, Dr. L. Bertini, Dr. C. Gatti
CNR-ISTM, Instituto di Scienze e Tecnologie Molecolari
via C. Golgi 19, 20133 Milano (Italy)
Fax: (+39) 2-50314300
E-mail: c.gatti@istm.cnr.it

Introduction

Outstanding thermoelectric properties have been reported for Zn–Sb alloys,[1] and in particular the compound Zn_4Sb_3 (formal stoichiometry) has caused a lot of excitement in the materials science community, due to its extremely high thermoelectric figure of merit at relatively moderate temperatures.[1] The complex phase diagram for Zn–Sb alloys is a matter of controversy and it was recently reinvestigated[2] since the thermoelectric properties of these alloys strongly depend on their specific phase and exact composition.[3] Caillat et al.[1] found a maximum thermoelectric figure of merit of 1.3 at 670 K for a p-type β-Zn_4Sb_3 sample, which appears to be a promising substitute for PbTe, due to its higher figure of merit, and it also has the advantage of

  DOI: 10.1002/chem.200400327

being lead free. The figure of merit is defined by Equation (1):

$$ZT = \alpha^2\sigma T/\kappa \quad (1)$$

in which α is the Seebeck coefficient, σ is the electrical conductivity, κ is the thermal conductivity and T is the absolute temperature.[4] The conversion efficiency for thermoelectric cooling or power generation increases monotonically with ZT. The Seebeck coefficient and electrical conductivity in Zn_4Sb_3 are not exceptionally high and the power factor, $\alpha^2\sigma$, is only half that of optimally doped $(Bi,Sb)_2Te_3$. It is the unusually low lattice part of the thermal conductivity (κ_L) that gives a very high ZT. In a recent single-crystal X-ray diffraction study we showed that the very low κ_L can be explained by the existence of amorphous-like, interstitial zinc atoms inside the rigid crystalline lattice.[5] The discovery of the interstitial Zn atoms finally gave a crystal structure of Zn_4Sb_3 in accordance with the measured mass density, which has been an evident problem for previously published structures.[6] The interstitial Zn atoms provide a novel scattering mechanism for phonons and also provide an explanation for the observed crystal chemistry.[5] The interstitial Zn atoms should also affect the electronic structure and transport properties of Zn_4Sb_3. A previous first-principles study[7] of β-Zn_4Sb_3 was based on the then available crystal structure[6] which assumed a mixed Zn-Sb occupancy site to comply with the experimental composition, $Zn_{6.33}Sb_{4.77}$, and which did not reveal any Zn interstitial atoms. By using a highly symmetrical model structure, Zn_6Sb_5 stoichiometry and a rigid band approach to reproduce the experimentally observed transport properties, Zn-Sb was theoretically described[7] as a low-carrier density metal with a remarkably high Seebeck coefficient for a metallic material.

In this study, we have determined the X-ray electron density of Zn_4Sb_3 from a combined Rietveld/maximum entropy method (MEM) analysis of synchrotron radiation powder diffraction data.[8] In our previous study, conventional single-crystal data were analysed by standard least-squares modelling techniques.[5] However, owing to the presence of systematic errors such as absorption, extinction, anomalous scattering and slight twinning, the conventional single-crystal data were not suitable for high-quality MEM reconstruction. The MEM has in recent years provided insights into the structures and chemical bonding of, for example, metallofullerenes and nanoporous solids.[9] However, the limitation of the method in these studies clearly has been that visualisation of the thermally smeared total electron density only provides qualitative information. In this study a new computer program InteGriTy[10] was used to carry out full Bader topological analysis[11] of the thermally smeared electron density obtained by the MEM and it is shown that important new information can be obtained by this method.[12] This greatly enhances the potential for extracting useful chemical and physical information from MEM electron densities. Based on the MEM density we then used an ab initio computational approach to deconvolute structural information from the space-time data averaging inherent to the XRD experiment. This enabled us to unravel whether and how interstitial and vacant Zn atoms affect the electronic structure and transport properties of β-Zn_4Sb_3. Such an insight into the peculiar features of this promising thermoelectric material is only made possible by the discovery of Zn interstitial atoms which were not known when the previous theoretical study was performed.

Experimental Section

Synchrotron powder diffraction: High-resolution synchrotron powder diffraction data were collected at a short wavelength ($\lambda = 0.42061$ Å) in a 0.1 mm capillary at beam line BL02B2 at SPring8, Figure 1. Room temperature measurements were carried out using a large Debye–Scherrer camera with an image plate detector.[13] The incident X-ray wavelength was determined by calibration with a standard CeO_2 sample ($a = 5.411102$ Å). The image plates were scanned with a pixel resolution of 50 μm. The data extend from $2\theta = 3$–$39°$ with a step size of 0.01° ($d_{min} = 0.626$ Å). A total of 94 parameters were fitted with full pattern Rietveld refinement to 3621 data points (structure 39, scale 1, profile 8, peak shift 2, background 44). The space group is $R\bar{3}c$ (167) with $a = 12.22320(4)$ and $c = 12.41608(7)$ Å.

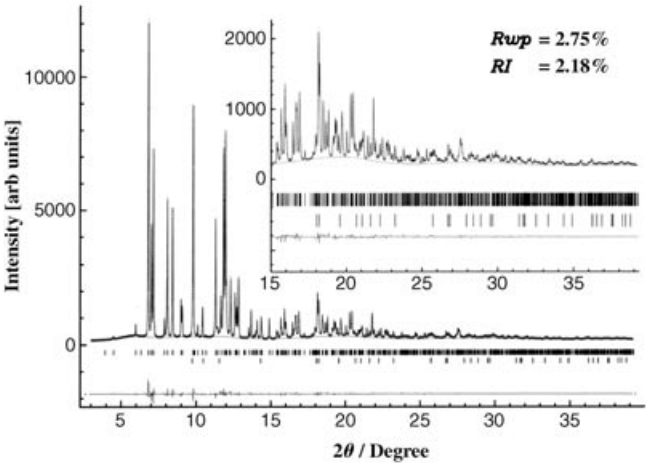

Figure 1. Synchrotron radiation powder diffraction data of Zn_4Sb_3. The difference between observed and calculated data are shown at the bottom of the plot.

Combined Rietveld/maximum entropy method analysis: The details of the combined Rietveld/MEM analysis of powder diffraction data have been presented extensively in the literature.[8] Basically MEM calculations use scaled, phased, "error free" structure factors as input for finding the numerical grid density (ρ_x) that optimises S [Eq. (2)] subject to the constraints of the data given by Equation (3).[14]

$$S = -\rho_x \log(\rho_x/\tau_x) \quad (2)$$

$$\chi^2 = 1/N \sum (F_o - F_c/\sigma(F_o)) = 1 \quad (3)$$

Conventional Rietveld modelling is used to extract structure factors from the synchrotron powder diffraction data and the starting point for the analysis described in this work was a structural model without interstitial atoms consisting only of a rigid crystal lattice.[5] As explained by Snyder et al.[5] the structural model with disorder between Zn and Sb at site 18e in space group $R\bar{3}c$ (167) published by Mayer et al.[6] is clearly incorrect when refined against new single-crystal data. For the single-crystal data the crystallographic R factor drops from 4.3% to 3.9% when changing the Zn occupancy at site 18e from 11% (Mayer et al. model) to 0%. From the initial refinement without Zn interstitial atoms, structure fac-

tors were extracted for MEM calculations and the corresponding electron density revealed several positions of interstitial atoms. The largest interstitial peak was included in a new Rietveld model and the structure factor extraction and MEM procedure were repeated. In the following two Rietveld/MEM cycles a total of three interstitial sites found in the MEM density were added to the Rietveld model. In the refinement of the powder data a small impurity phase of metallic Zn was also observed. The final residual parameters for the model with three interstitial atoms were $R_P=0.0203$, $R_{wP}=0.0268$, $R_F=0.0237$, $R_F(\mathrm{MEM})=0.0215$ (for 802 reflections with $d_{min}=0.626$ Å), see Table 1. This is a significant improvement compared with the model without interstitial atoms ($R_P=0.0326$, $R_{wP}=0.0446$, $R_F=0.0394$, $R_F(\mathrm{MEM})=0.0290$). Some of the refined interatomic distances are quite short (Zn2–Zn2 = 1.85 Å, Zn2–Zn3 = 2.07 Å), but since X-ray diffraction measures the average crystal structure, the interstitial atoms are not all necessarily present in the same unit cell. Nevertheless, we have refined a model with a restraint of 2.25 Å on the Zn–Zn distances ($R_P=0.0206$, $R_{wP}=0.0275$, $R_F=0.0229$, $R_F(\mathrm{MEM})=0.0218$), Table 1.[15] There is virtually no difference in the structure factor extraction from the powder data in the restrained and nonrestrained models and the subsequent MEM density is therefore also insensitive to the two final Rietveld models. The MEM density discussed below refers to the restrained Rietveld model. The most important point is that the diffraction data shows beyond doubt the existence of interstitial sites in Zn_4Sb_3; the final crystal structure is shown in Figure 2. The interstitial positions found in the analysis of the synchrotron powder data are in excellent agreement with the interstitial positions found in the Fourier analysis of conventional single-crystal data.[5] This shows that the three interstitial sites are inherent to the structure of Zn_4Sb_3, since the single crystal and the powder were synthesised by different methods. The stoichiometry of the model with three interstitial atoms is $Zn_{38.45}Sb_{30}$ and the calculated density is in excellent agreement with the measured value (6.37 versus 6.36 g cm^{-3}).[5]

Table 1. Atomic coordinates and equivalent isotropic parameters [$10^4\times$Å^2] for models of Zn_4Sb_3.[a]

Atom	Site	*X*/*a*	*Y*/*b*	*Z*/*c*	Occupancy	U_{iso}
Zn(1)	36f	0.07944(4)	0.24481(6)	0.40260(5)	0.894(1)	307(4)
A		0.07915(4)	0.24483(6)	0.40273(5)	0.899(1)	268(4)
		0.0792	0.2444	0.4025	0.898	
Sb(1)	18e	0.35586(3)	0.0	0.25	1	155(2)
		0.35559(3)	0.0	0.25	1	152(2)
		0.3554	0.0	0.25		
Sb(2)	12e	0.0	0.0	0.13621(2)	1	174(3)
		0.0	0.0	0.13646(2)	1	174(3)
		0.0	0.0	0.1363		
Zn(2)	36f	0.1684(8)	0.432(1)	0.063(1)	0.059(1)	821
B		0.1782(8)	0.434(1)	0.030(1)	0.068(1)	1253(113)
		0.1827	0.4344	0.041	0.067	
Zn(3)	36f	0.2394(7)	0.4494(8)	0.1976(3)	0.059(1)	402
C		0.2391(7)	0.4553(8)	0.2093(3)	0.068(1)	317(25)
		0.2385	0.4534	0.2058	0.056	
Zn(4)	36f	0.117(1)	0.231(1)	0.268(1)	0.054(1)	1252
D		0.131(1)	0.233(1)	0.278(1)	0.033(1)	127(38)
		0.1302	0.2310	0.2770	0.026	

[a] The first line refers to the unrestrained Rietveld model and the second line to the restrained Rietveld model. The third line gives the position of the density maxima found by topological analysis of the MEM density. The topological occupancies for Zn are obtained by dividing the total number of electrons integrated over the atomic volume by the atomic number of Zn (30).

It is generally believed that single-crystal data are more accurate than powder data. While this undoubtedly is true in many cases, it is not necessarily so for high-symmetry inorganic crystal structures containing heavy elements. Such crystals often have substantial absorption and anomalous scattering effects at the wavelengths used in conventional single-crystal X-ray diffractometers ($Mo_{K\alpha}$). Furthermore, extinction effects can be severe in low-order data due to a high degree of crystal perfection. In the present case of Zn_4Sb_3 there may also be an additional problem of subtle twinning.[5] It was for these reasons we decided to collect short-wavelength synchrotron powder data in a very thin capillary (0.1 mm). Simulation of absorption effects in our powder data predict that they are less than 1% in high-order data (i.e., negligible). Owing to the combined use of a powder sample and short wavelength, extinction effects are also suppressed and the powder furthermore takes care of potential twinning. Finally, anomalous scattering is minimised by the use of a short wavelength. Overall, the synchrotron powder data are therefore expected to be more accurate than the conventional single-crystal data, and this is indeed confirmed by comparison of the MEM densities obtained with the two data sets.

In least-squares analysis, systematic errors are to some extent removed since they are not fitted by the model, and just lead to higher residual factors. MEM analysis uses the structure factors at face value and thus has no "filter" to remove systematic discrepancies in the data.[16] For this reason the quality of the data is critical in quantitative MEM calculations. In Figure 3 we compare the MEM density obtained from the synchrotron powder data with the MEM density calculated from the conventional single crystal.[5] The two data sets have similar resolutions: 0.63 Å for the powder data versus 0.57 Å for the single-crystal data. The coarse (atomic) features of the two densities are virtually identical, but the powder density is much less noisy. As an example, plots of the radial distributions of the atomic densities (data not shown) show that the single-crystal density is full of small spikes, whereas the powder density smoothly decays away from the nucleus. Noise in MEM maps is an effect of small uncorrected systematic errors,[16] and therefore we have used the powder density in further analysis.

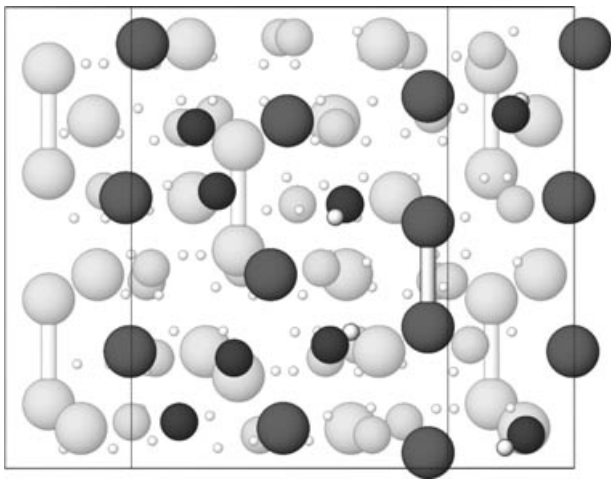

Figure 2. The crystal structure of Zn_4Sb_3 including three interstitial Zn sites (small spheres). Sb atoms are shown as large spheres and Zn atoms on the main lattice site are shown as medium-sized sphere. Atoms in or near the plane of Figure 3 are highlighted.

Computational methods: We performed fully periodic density functional theory (DFT) computations using the CRYSTAL98[17] suite of programs and the B3PW91 exchange-correlation functional.[18] The core electrons of both Zn and Sb atoms are described by the large core pseudo-potentials (PP) developed by Hay and Wadt.[19] Within this approach the zinc

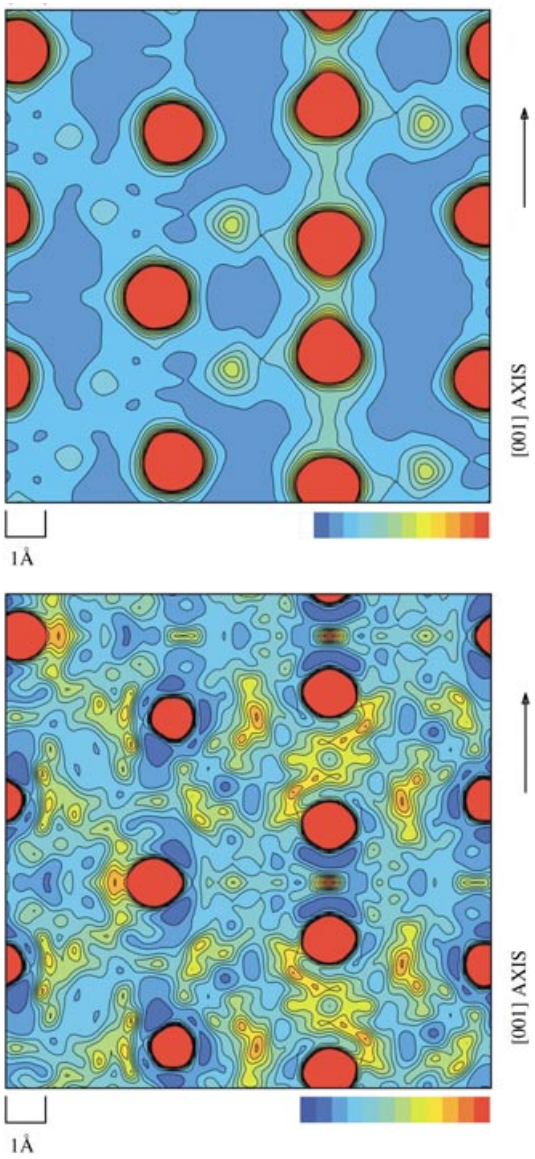

Figure 3. Contour plot of the MEM density in the Sb_2^{4-} dimer region. The contour level is 0.2 e Å^{-3}. Top: The density obtained from synchrotron powder data. Bottom: The density obtained from conventional single-crystal data.

atoms have 12 active electrons each ($3d^{10}4s^2$ electronic configuration), while each antimony atom has five active electrons ($5s^25p^3$ configuration). The original double-zeta basis set provided by Hay and Wadt to be used in conjunction with the selected PPs was designed for molecular computations. Therefore, we had to introduce minor changes into the original basis set to obtain a suitable wavefunction for crystals. Finally, from this slightly modified basis (the *reference basis*) we derived a new basis set (the *final basis*) that saves 90% of CPU time without introducing significant changes into the electronic structure of the material. The final basis set is the same size as the reference set (Zn: 2s1p2d; Sb: 2s2p), but adopts the s = p constraint for the outermost shell of Zn and uses modified Gaussian contraction coefficients and exponents. The quality of the final basis set was judged against that of the reference basis by comparing 1) the density of states (DOS) and their atomic projections around the Fermi level and 2) Bader atomic charges[11] by using the TOPOND-98 package.[20] The DOS obtained with the two basis sets are hardly distinguishable and Bader's net charges differ by 0.14 e at the utmost. These preliminary computations were carried out on an $R\bar{3}c$ cell and on a $Zn_{12}Sb_{10}$ structure without interstitial atoms or defects, since the Zn atoms at the main site recover about 85% of the overall zinc content. Defective systems (i.e., crystals containing interstitial atoms and/or vacancies) have been simulated by introducing a defect into each cell in order to preserve the translational symmetry of the system.

The Seebeck coefficient, α, was calculated using the code ELTRAP[21] based on the semi-classical one-electron Boltzmann transport theory,[22] as used by Blake et al.[23] Since we assumed a constant relaxation time for each wave-vector and band index, the α values could be calculated from first principles knowing only the band structure. The numerical integration in **k** space was performed in the irreducible wedge of the first Brillouin zone using a total of 20^3 **k** points. For each system, we considered 21 bands around the Fermi level, nine of which are below and the remaining 12 above this level.

Results and Discussion

Topological analysis of the MEM density: The crystal structure containing interstitial Zn has profound implications for understanding Zn_4Sb_3, which may now be considered a Zintl phase. Based on bonding distances there are 18 free Sb^{-3} ions (Sb1) and six $(Sb_2)^{-4}$ dimers (Sb2) in the unit cell, which requires a total donation of 78 electrons from the Zn atoms. Thus, 39 Zn atoms of valence +2 are required for charge balance. This is close to the stoichiometry of the present model. A very important question is whether the MEM density provides evidence for the formal charge counting and the Zintl model. Figure 3 (top) shows a contour map in the plane of the proposed Sb–Sb dimer bond. The MEM density in the dimer does indeed show a build up of covalent density between the Sb atoms as anticipated if the atoms form a dimer. In contrast, the electron density of the Sb1 atom is more spherical. If the structure had been well ordered without interstitial Zn sites it would be straightforward to carry out charge integration over the atomic basins to quantify the differences in charge between the two Sb sites. However, it is difficult to determine atomic volumes when the density contains many superimposed features (time and space average). We have carried out Bader topological analysis of the numerical MEM grid density using a newly developed software program InteGriTy.[10] A thorough critical-point search establishes six maxima corresponding to two Sb atoms and one Zn atom, which form the basic crystal structure, and three Zn interstitial atoms. Apart from the Zn2 site (0.15 Å), the topological maxima locations are found to be close to the Rietveld refined positions of the restrained model (less than 0.002 Å for Sb1 and Sb2, 0.01 Å for Zn1 and 0.03 Å for Zn3 and Zn4). The position found for the Zn2 site gives a quite short Zn2–Zn3 contact of 2.13 Å. We furthermore located a small maximum on the "back side" of the Sb atom in the dimer along the *c* axis (0,0,0.0241). This non-nuclear maximum (NNM) is quite intriguing. The atomic basins, as defined from the gradient vector field of the electron density, for the different types of atoms are shown in Figure 4. The plot consolidates the observation from the total density that the Sb atoms indeed have very different volumes and charge distributions. The atomic volume of the NNM fits perfectly into a void in the Sb2 atomic volume along the *c* axis. The NNM suggests that Zn_4Sb_3 may in fact also exhibit Sb disorder along the *c* axis, reminiscent of a chain of dimers in which the Sb–Sb bond

Figure 4. Atomic surfaces defined by the zero flux condition of the different atoms in the Zn_4Sb_3 structure viewed nearly along the *c* axis. The light shiny green basins along the *c* axis correspond to the "dimer" Sb atom. At the top of the Sb dimer a non-nuclear maxima (blue) fits exactly into the void. The red basin is the main Zn atom, the purple basins are the interstitial Zn atoms and the matt green basin is the Sb^{3-} ion.

for a given atom can point in either direction. Analogous to this is a lattice of hydrogen atoms that undergoes a Peierls distortion to form H_2 molecules.[24] The (3,−1) bond critical points are located between the Sb atoms in the dimer, but also between Sb and the NNM, and between the NNM themselves. An alternative explanation of the NNM could be that the dimer bonds in some unit cells are broken leading to two isolated Sb^{3-} ions. However, this would increase the charge required from the Zn^{2+} ions to provide charge balance. No matter what, the subtle Sb disorder must contribute to a further reduction in the thermal conductivity. It may be argued that the NNM could correspond to interstitial atoms, but this is unlikely since the Sb sites are fully occupied and the Sb to NNM distance is very short.

In Table 2 we list the integrated atomic properties of the two Sb atoms, the NNM and the four Zn atoms. Adding the atomic populations gives 2646.2 electrons for the entire unit cell compared with the pixel count of 2649.4 electrons. The corresponding sum of atomic volumes is 1554.8 $Å^3$ compared with a unit cell volume of 1586.6 $Å^3$. Hence the topological analysis of the grid density is indeed very accurate and retrieves all the features even in the case of a space- and time-averaged density containing superimposed atoms. The topological analysis also confirms that the MEM density obtained from synchrotron powder data is very smooth with little noise in the valence regions—a fingerprint of high data quality. The observed Bader charges are less than expected from the qualitative structural interpretation, but the Zn atom populations are in good agreement with the refined occupation factors of the Rietveld model. The integrated charge on the Zn1 site corresponds to an occupation of 0.898. This is strong nonbiased evidence for the proposed partial occupancy model of this site in contrast to previous models in which the main Zn site is fully occupied.[6]

Table 2. Integrated properties of Bader topological atoms in the MEM density of Zn_4Sb_3.

	Atomic volume [$Å^3$]	Electronic population
Sb1	136.38	49.44
Sb2	146.43	51.42
NNM	4.96	0.31
Zn1	83.74	26.94
Zn2	43.99	2.01
Zn3	21.26	1.67
Zn4	22.14	0.78

Electronic structure: In theoretical modelling, we start with the X-ray structure and use an ab initio computational approach to deconvolute structural information from the space–time data averaging inherent to the XRD experiment. This enables us to unravel whether and how interstitial and vacant Zn atoms affect the electronic structure and transport properties of β-Zn_4Sb_3. We have not addressed the effect of the possible subtle disorder of Sb atoms along the *c* axis. In the following discussion we switch to the trigonal setting of the $R\bar{3}c$ space group. Here antimony atoms are sited in the 6e and 4c positions with unit occupancy, while the zinc atoms are distributed with fractional occupancies over four 12f positions, from now on denoted by the letters A–D (Table 1). The overall stoichiometry of the distance-restrained Rietveld model is $Zn_{12.816}Sb_{10}$, which is zinc-deficient with respect to the 4:3 ratio. If we label zinc atoms by their crystallographic special positions, the cell stoichiometry assumes the expression $A_{10.788}B_{0.816}C_{0.816}D_{0.396}Sb_{10}$, which corresponds to the following occupancies: A = 0.899, B = 0.068, C = 0.068 and D = 0.033, Table 1.

To recover snapshots of the instantaneous local structure within individual crystal cells and to relate them to the electronic properties of the material, we performed an extensive theoretical investigation of a large set of different crystal structures. The four simplest structures, $X_{12}Sb_{10}$ (X = A, B, C or D), belong to the $R\bar{3}c$ space group and have unit occupancy of one of the four available 12f special positions. The $A_{12}Sb_{10}$ unit cell is by far the most stable of these structures (by over 200 kcal mol^{-1} $cell^{-1}$, see Table 3), in good agreement with the dominant occupation of the 12f special position A. We therefore assumed that the overall structure is made up of $A_{12}Sb_{10}$ cell domains containing B, C and D atoms as point or possibly extended defects. The $X_{12}Sb_{10}$ crystals have the electronic structure of highly p-doped semiconductors. The DOS of $A_{12}Sb_{10}$ are shown in Figure 5 and the local environment around zinc is shown in Figure 6.

Table 3. Relative energies of the $X_{12}Sb_{10}$ (X = A, B, C, D) structures.

Stoichiometry	Relative energy[a]	Stoichiometry	Relative energy[a]
$A_{12}Sb_{10}$	0	$B_{12}Sb_{10}$	+210
$C_{12}Sb_{10}$	+325	$D_{12}Sb_{10}$	+324

[a] Defined as $[E(X_{12}Sb_{10})-E(A_{12}Sb_{10})]$ and expressed in kcal mol^{-1} $cell^{-1}$.

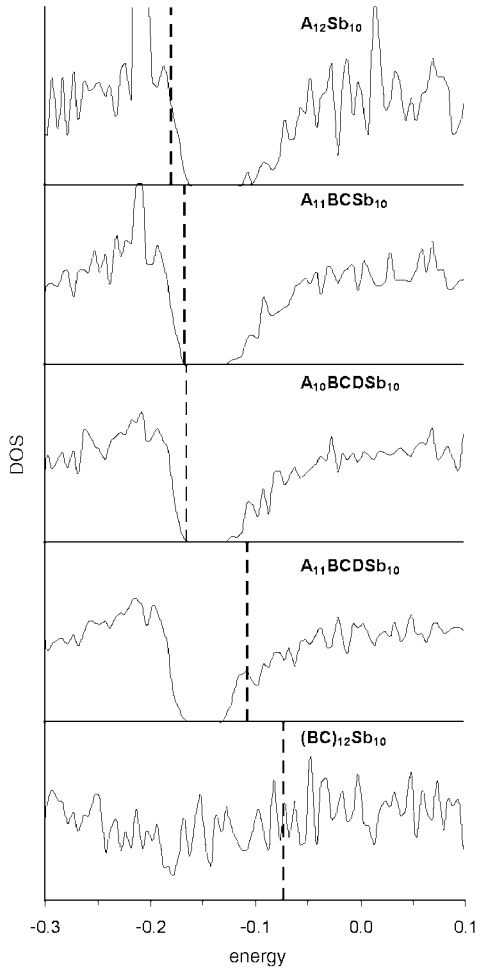

Figure 5. Density of states (DOS) of the zinc antimonide cells. The structures (except for $(BC)_{12}Sb_{10}$) have similar DOS up to 14 Zn atoms per cell and their electronic properties are primarily determined by the different electron filling that occurs as the number of zinc atoms increases. Energy is given in hartrees and DOS in arbitrary units. The Fermi level is indicated by a dashed line.

The experimental Zn to Sb ratio, that is, about 1.28, could be easily interpreted as a 1:4 mixture of cells containing 12 and 13 zinc atoms, respectively. However, $A_{12}Sb_{10}$ cells as such cannot host any interstitial zinc atom, since every $A_{12}XSb_{10}$ (X = B, C or D) structure implies that the Zn–Zn internuclear distances are too short.[25] On the other hand, if a zinc vacancy is created in $A_{12}Sb_{10}$, it is then possible to build up seven point defects using the three different zinc sites: $A_{11}BSb_{10}$, $A_{11}CSb_{10}$ and $A_{11}DSb_{10}$, which have $Zn_{12}Sb_{10}$ stoichiometry, $A_{11}BCSb_{10}$, $A_{11}BDSb_{10}$ and $A_{11}CDSb_{10}$ with $Zn_{13}Sb_{10}$ stoichiometry and $A_{11}BCDSb_{10}$ with $Zn_{14}Sb_{10}$ stoichiometry. The ternary structures ($A_{11}X_1Y_1Sb_{10}$) are preferred to a combination of binary ($A_{11}X_1Sb_{10}$) and quaternary ($A_{11}BCDSb_{10}$) ones, since the reactions given in Equations (4)–(6) are all highly exothermic (−100, −105 and −110 kcal mol^{-1}, respectively).[26]

$$A_{11}BSb_{10} + A_{11}BCDSb_{10} \rightarrow A_{11}BCSb_{10} + A_{11}BDSb_{10} \quad (4)$$

$$A_{11}CSb_{10} + A_{11}BCDSb_{10} \rightarrow A_{11}BCSb_{10} + A_{11}CDSb_{10} \quad (5)$$

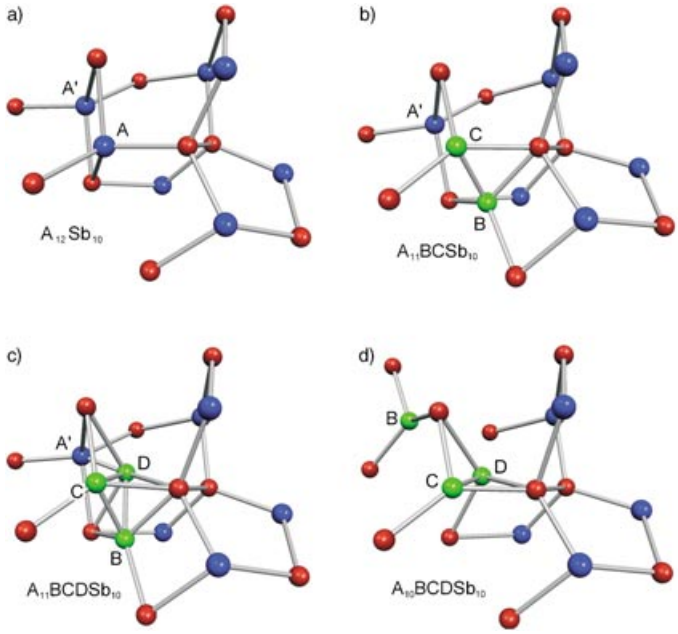

Figure 6. Interstitials and vacancies in zinc antimonide. Sb atoms (red), Zn atoms (blue) and Zn interstitials (green). a) The nondefective 12-Zn atom structure; b) an A vacancy is created and the BC dimer is inserted to yield a 13-Zn atom structure; c) a third interstitial, D, is inserted to form a 14-Zn atom structure; d) a second vacancy is created by removing A′ and by allowing BCD atoms to rearrange to the most stable $A_{10}BCDSb_{10}$ system (a 13-Zn atom structure).

$$A_{11}DSb_{10} + A_{11}BCDSb_{10} \rightarrow A_{11}BDSb_{10} + A_{11}CDSb_{10} \quad (6)$$

The structures considered up to now have very similar DOS (see Figure 5) regardless of the zinc content and structure. Therefore, their electronic properties depend primarily on the number of available valence electrons. $A_{12}Sb_{10}$ has the structure of a p-doped semiconductor and the same holds true for all binary defects. The ternary structures are nondoped semiconductors and the quaternary structure is an n-doped semiconductor. Since the rigid band approximation is satisfied to a high degree in this system, hypothetical 1:4 mixtures of cells with $Zn_{12}Sb_{10}$ and $Zn_{13}Sb_{10}$ stoichiometry should behave as a lightly p-doped material, in agreement with experiment.[1]

$A_{11}BCSb_{10}$ is the most stable of the ternary defects, as shown in Table 4. This outcome is in agreement with the experimental observation that the B and C positions are more occupied than D. This also justifies the occupancy of these two zinc sites being constrained to be equal in the refinement of the synchrotron powder data, Table 1. The experimental and theoretical data together strongly indicate that the atoms in the B and C positions form a zinc dimer (B–

Table 4. Relative energies of the $A_{11}XYSb_{10}$ *ternary* defects.

Stoichiometry	Relative energy[a]	Stoichiometry	Relative energy[a]
$A_{11}BCSb_{10}$	0	$A_{11}BDSb_{10}$	+32
$A_{11}CDSb_{10}$	+19		

[a] Defined as $[E(A_{11}XYSb_{10}) - E(A_{11}BCSb_{10})]$ and expressed in kcal mol^{-1} cell^{-1}.

C = 2.23 Å, see Figure 6) that replaces one atom in the A position in $A_{12}Sb_{10}$ cells. To evaluate whether BC dimers cluster in extended domains, we substituted all the A atoms of an $A_{12}Sb_{10}$ cell with BC couples. From the energy gain of the reaction given in Equation (7), it is evident that BC dimers must be considered as point defects.

$$(BC)_{12}Sb_{10} + 11A_{12}Sb_{10} \rightarrow 12A_{11}BCSb_{10} \qquad \Delta H = -1186\,\text{kcal mol}^{-1} \tag{7}$$

We obtained analogous results with the $(CD)_{12}Sb_{10}$ structure, which strengthens this conclusion.[27] Moreover, $(BC)_{12}Sb_{10}$ and $(CD)_{12}Sb_{10}$ crystals have a metallic band structure (see Figure 5), in disagreement with experimental findings.[28]

Let us now assume that the crystal is made up of a mixture of $A_{12}Sb_{10}$ and $A_{11}BCSb_{10}$ cells, such as to reproduce the experimental content of B and C atoms. This material would present an excess of A type atoms (0.396 atoms cell^{-1}) and an equivalent deficiency of D atoms with respect to the experimental stoichiometry. To reproduce the experimental occupancies it is thus necessary to insert D atoms (I_D) while creating A vacancies (V_A) in the $A_{12}Sb_{10}$ and $A_{11}BCSb_{10}$ cells. We generated all the possible structures within the constraint of the Zn–Zn internuclear distance threshold.[25] The energy changes due to the insertion of the defects are reported in Table 5. First I_D and V_A must coexist in the same cell, otherwise the energy requested for introducing them as separate entities would be inaccessibly high (178 kcal mol^{-1} cell^{-1}). Secondly, substitution of A by D in ideal $A_{12}Sb_{10}$ cells is less preferable than the insertion of $I_D + V_A$ into the already defective $A_{11}BCSb_{10}$ structure to give $A_{10}BCDSb_{10}$.[29] The latter structure has 44 possible nonequivalent geometrical conformations; the most stable one (see Figure 6) is nearly degenerate with respect to the original $A_{11}BCSb_{10}$ cell and nearly has an equivalent electronic structure (see Figure 5). It appears that D atoms are not isolated substitutional defects randomly distributed within the material, but rather they represent a Zn atom lying in the proximity of the BC dimer and which has been displaced from special position A to special position D. Experimentally there is about one D atom for every two BC dimers, consistent with the quasidegeneracy of $A_{11}BCSb_{10}$ and the most stable $A_{10}BCDSb_{10}$ cell.

Table 5. Energy changes ΔE for the insertion of $(I_D + V_A)$[a] in the $A_{12}Sb_{10} + A_{11}BCSb_{10}$ cells.

Final products	ΔE[b]
$A_{11}DSb_{10} + A_{11}BCSb_{10}$	+55
$A_{11}Sb_{10} + A_{11}BCDSb_{10}$	+178
$A_{12}Sb_{10} + A_{10}BCDSb_{10}$	$+7 \le \Delta E \le +144$[c]

[a] See text for details. [b] Defined as $[E(\text{products}) - E(A_{12}Sb_{10} + A_{11}BCSb_{10})]$ and expressed in kcal mol^{-1} cell^{-1}. [c] Since $A_{10}BCDSb_{10}$ has 44 nonequivalent arrangements, the overall energy range is reported.

In summary, we propose that zinc antimonides consist of an ideal $A_{12}Sb_{10}$ framework in which point defects are distributed. Atoms in the B and C positions couple to form dimers that occupy the cavity of a single A vacancy, with clustering of dimers being disfavoured. Atoms in the D position reveal that the BC dimers possibly induce a rearrangement in the surrounding framework by displacing zinc atoms from the A to D positions to yield more complex structures (see Figure 6) of similar energies.[29] The experimental stoichiometry is exactly reproduced, assuming that the material is a 0.184:0.420:0.396 mixture of $A_{12}Sb_{10}$, $A_{11}BCSb_{10}$ and $A_{10}BCDSb_{10}$ cells, respectively. Cells with zinc content higher than 13 atoms are not competitive in terms of energy considerations.

As concerns the electronic structure of the material, crystal cells with 12–14 zinc atoms display nearly equivalent DOS (see Figure 5) and their properties are essentially determined by the different electron filling that occurs as the number of zinc atoms increases. Crystals with $Zn_{12}Sb_{10}$ stoichiometry are semiconductors with a p-doping level of two electrons per cell as obtained by integrating the DOS from the Fermi level energy up to the band gap. Insertion of another zinc atom into the cell completely fills the states lying in this energy range. The addition of further zinc atoms ($Zn_{14}Sb_{10}$) corresponds to n-doping. Finally $(BC)_{12}Sb_{10}$ or $(CD)_{12}Sb_{10}$ cells are metallic.

Given the similar DOS of the $A_{12}Sb_{10}$, $A_{11}BCSb_{10}$ and $A_{10}BCDSb_{10}$ cells, we can electronically model (Figure 7) the defective stoichiometry of the real system either by n-doping the 12-Zn atom cell (n) or by p-doping one of the two 13-Zn atom cells ($p1$, $p2$). By adding $(12.816-12)\times 2e/Zn = 1.632$ e to $A_{12}Sb_{10}$ or removing $(13-12.816)\times 2e/Zn = 0.368$ e from either $A_{11}BCSb_{10}$ or $A_{10}BCDSb_{10}$ similar calculated positive Seebeck coefficients (115.0, 123.0 and 110.3 μV K^{-1}, respectively, at $T = 670$ K) are obtained, which confirms that the DOS of these systems are actually similar to each other and that the defective system is a p-doped semiconductor, as found experimentally.[1] The effect on the electronic transport properties is dramatic when these cells are doped differently with respect to the electron count of $12.816 \times 2e$.

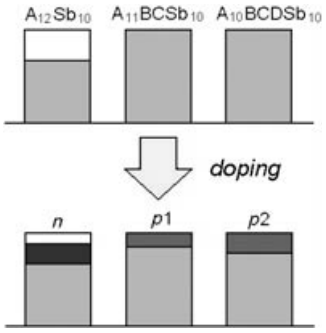

Figure 7. The electronic structure of $Zn_{12.816}Sb_{10}$. Given the similar DOS of the $A_{12}Sb_{10}$, $A_{11}BCSb_{10}$ and $A_{10}BCDSb_{10}$ cells, the defective stoichiometry of the real system can be modelled either by n-doping the 12-Zn atom cell or by p-doping one of the two 13-Zn atom cells. Alternatively one may calculate the set of n, $p1$ and $p2$ values so that the chemical potential of the three structures are equal, under the appropriate stoichiometric constraints (see text).

The Seebeck coefficient will increase by adding extra electrons to either kind of cells. For example, adding 0.33 electrons, a doping which still preserves the p-doped character of the cells, yields a Seebeck coefficient of about 260 $\mu V K^{-1}$ for the three cells. However, additional electrons will generally also lower σ, so the effect on Z [Eq. (1)] is not certain. Indeed, optimal $\sigma^2\sigma$ values are computationally found when 0.168, 0.068, 0.118 extra electrons are added to $A_{12}Sb_{10}$, $A_{11}BCSb_{10}$ and $A_{10}BCDSb_{10}$, respectively, with corresponding Zn contents equal to 12.9, 12.85 and 12.875.

Alternatively, one may model the defective system by retaining the 0.184:0.420:0.396 mixture of $A_{12}Sb_{10}$, $A_{11}BCSb_{10}$ and $A_{10}BCDSb_{10}$ cells and by n-doping the 12-Zn atom cell and p-doping the 13-Zn atom cells so that the chemical potential of the three systems are equal at a given temperature. Also by imposing the constraint of the total electron count implied by the $Zn_{12.816}Sb_{10}$ stoichiometry, one obtains n, $p1$ and $p2$ (Figure 7) values equal to 1.237, 0.192 and 0.366 e, respectively, at $T = 670$ K. The associated Seebeck coefficients turn out to be 76.7, 160.4 and 110.6 $\mu V K^{-1}$.

In the real system, the bands of $A_{12}Sb_{10}$, $A_{11}BCSb_{10}$ and $A_{10}BCDSb_{10}$ cells are modified to give a unique band structure. This should redistribute electrons among the three cells to yield a slightly different set of n, $p1$ and $p2$ values at chemical equilibrium. Since the electronic transport properties of the $Zn_{12.816}Sb_{10}$ system appear to be extremely sensitive to changes in doping of the 12-Zn and 13-Zn atom cells, this electron redistribution could significantly change the thermoelectric properties of the composite material.[30]

Conclusions

We have determined the experimental electron density of the high-performance thermoelectric material Zn_4Sb_3 based on accurate short-wavelength synchrotron powder diffraction data. Analysis of the MEM electron density provides a solid foundation for the proposed crystal chemistry and directly reveals interstitial Zn atoms. Two types of Sb atoms are observed corresponding to a free spherical ion (Sb^{3-}) and Sb_2^{4-} dimers. The density features make it possible to rationalise the structure as a Zintl phase without assuming any specific structure for the interstitial sites. Overall the density contains one partially occupied main Zn site, three Zn interstitial sites and possible Sb disorder along the c axis. These are all features which contribute to the drastic reduction of the thermal conductivity of the material. Topological analysis of the thermally smeared MEM grid density was carried out. This approach can greatly enhance the power of MEM charge density analysis since topological analysis is a well-tested quantitative interpretation tool firmly rooted in quantum mechanics.

The subsequent structural analysis of the $Zn_{12.816}Sb_{10}$ system allows for a deeper understanding of its electronic transport properties and of the extreme sensitivity of these properties to subtle changes in the material's composition. It also suggests that the exciting thermoelectric properties reported for zinc antimonide can likely be even further improved. Finally, it demonstrates that the Zn interstitial atoms play a fundamental role as electron suppliers and Seebeck coefficient enhancers, as well as lattice thermal conductivity suppressors. Such a role could not have been explored in previous theoretical studies, since the Zn interstitial atoms had not then been discovered.

Acknowledgements

The Danish Research Councils are acknowledged for funding through the DANSYNC Center and for access to a 512-node PC cluster at the Danish Supercomputer Center, Southern Denmark University. E.N. thanks Prof. M. Sakata and Prof. M. Takata for valuable discussions. E.N. also thanks K. Kato for his experimental help at SPring-8. The synchrotron radiation experiments were performed at beam line BL02B2 at SPring-8 with the approval of the Japan Synchrotron Radiation Research Institute (JASRI). The work was supported in part by the European Community under Contract No. G5RD-CT2000-00292, NanoThermel project.

[1] T. Caillat, J.-P. Fleurial, A. Borshchevsky, *J. Phys. Chem. Solids* **1997**, *58*, 1119–1125.
[2] V. Izard, M. C. Record, J. C. Tedenac, S. G. Fries, *CALPHAD Comput. Coupling Phase Diagrams Thermochem* **2001**, *25*, 567–581.
[3] L. T. Zhang, M. Tsutsui, K. Ito, M. Yamaguchi, *J. Alloys Compd.* **2003**, *358*, 252–256.
[4] For papers on thermoelectrics see, for example: a) B. C. Sales, D. Mandrus, R. K. Williams, *Science* **1996**, *272*, 1325–1328; b) F. J. DiSalvo, *Science* **1999**, *285*, 703–706; c) A. Bentien, A. E. C. Palmqvist, J. D. Bryan, S. Latturner, G. D. Stucky, L. Furenlid, B. B. Iversen, *Angew. Chem.* **2000**, *112*, 3759–3762; *Angew. Chem. Int. Ed.* **2000**, *39*, 3613–3616; d) R. Venkatasubramanian, E. Siivola, T. Colpitts, B. O'Quinn, *Nature* **2001**, *413*, 597–602.
[5] G. J. Snyder, M. Christensen, E. Nishibori, T. Caillat, B. B. Iversen, *Nature Mater.* **2004**, in press.
[6] H. W. Mayer, I. Mikhail, K. Schubert, *J. Less-Common Met.* **1978**, *59*, 43–52.
[7] S.-G. Kim, I. I. Mazin, D. J. Singh, *Phys. Rev. B* **1998**, *57*, 6199–6203.
[8] For a review of the method, see: M. Takata, E. Nishibori, M. Sakata, *Z. Kristallogr.* **2001**, *216*, 71–86.
[9] a) M. Takata, B. Umeda, E. Nishibori, M. Sakata, Y. Saito, M. Ohno, H. Shinohara, *Nature* **1995**, *377*, 46–49; b) C. R. Wang, T. Kai, T. Tomiyama, T. Yoshida, Y. Kobayashi, E. Nishibori, M. Takata, M. Sakata, H. Shinohara, *Angew. Chem.* **2001**, *113*, 411–413; *Angew. Chem. Int. Ed.* **2001**, *40*, 397–399; c) R. Kitaura, S. Kitagawa, Y. Kubota, T. C. Kobayashi, K. Kindo, Y. Mita, A. Matsuo, M. Kobayashi, H. C. Chang, T. C. Ozawa, M. Suzuki, M. Sakata, M. Takata, *Science* **2002**, *298*, 2358–2361.
[10] C. Katan, P. Rabiller, C. Lecomte, M. Guezo, V. Oison, M. Souhassou, *J. Appl. Crystallogr.* **2003**, *36*, 65–73.
[11] R. F. W. Bader, *Atoms in Molecules: A Quantum Theory*, Oxford University Press, Oxford, **1990**.
[12] Topological analysis of thermally smeared MEM densities has been carried out on metallic beryllium: B. B. Iversen, F. K. Larsen, M. Souhassou, M. Takata, *Acta Crystallogr. Sect. B* **1995**, *51*, 580–592. In that study non-nuclear maxima were established for the first time in experimental charge density. Recently Merli and Camara used topological analysis of MEM densities in studies of mineral structures: M. Merli, F Camara, *Eur. J. Mineral.* **2003**, 15, 903–911.
[13] E. Nishibori, M. Takata, K. Kato, M. Sakata, Y. Kubota, S. Aoyagi, Y. Kuroiwa, M. Yamakata, N. Ikeda, *Nucl. Instrum. Methods Phys. Res. Sect. A* **2001**, 467, 1045–1048.
[14] The program ENIGMA (H. Tanaka, M. Takata, E. Nishibori, K. Kato, T. Iishi, M. Sakata, *J. Appl. Crystallogr.* **2002**, *35*, 282–286) was used for parallel code MEM calculations at the Danish Supercomputer Center. The calculations employed uniform priors and a $240\times240\times240$ pixel grid. Iterations were stopped at $\chi^2 = 1$. In the equations for S and χ^2, τ_x is the prior (start) density and N is the

number of observations. F_o and F_c are the observed and calculated structure factors, respectively.

[15] The restraint distance of 2.25 Å was determined from a series of refinements in which the distance restraint on the Zn–Zn contacts was increased in steps between 2.0 and 2.5 Å. A minimum in the Rietveld refinement reliability factors was found for 2.25 Å. There is no reference to a Zn dimer in the literature, but Hg and Cd dimers are well known: F. A. Cotton, G. Wilkinson, C. A. Murillo, M. Bochman, *Advanced Inorganic Chemistry*, 6th ed., Wiley, New York, **1999**. For Cd the dimer is 0.5 Å shorter than the Cd–Cd distance in the corresponding metal (2.5 versus 3.0 Å). Since the Zn–Zn distance in the metal is 2.67 Å, the choice of 2.25 Å seems reasonable. In the structure Zn2 and Zn3 form a chain and the two sites were constrained to identical occupancy.

[16] a) B. B. Iversen, S. K. Nielsen, F. K. Larsen, *Philos. Mag. A* **1995**, 72, 1357–1380; b) B. B. Iversen, J. L. Jensen, J. Danielsen, *Acta Crystallogr. Sect. A* **1997**, *53*, 376–387..

[17] V. R. Saunders, R. Dovesi, C. Roetti, M. Causà, N. M. Harrison, R. Orlando, C. M. Zicovich-Wilson, CRYSTAL98 User's Manual, University of Torino, Torino (Italy), **1998**.

[18] a) A. D. Becke, *J. Chem. Phys.* **1993**, *98*, 5648–5652; b) J. P. Perdew, Y. Wang, *Phys. Rev. B* **1989**, *40*, 3399–3399.

[19] a) W. R. Wadt, P. J. Hay, *J. Chem. Phys.* **1985**, *82*, 284–298; b) P. J. Hay, W. R. Wadt, *J. Chem. Phys.* **1985**, *82*, 299–310.

[20] C. Gatti, TOPOND98 User's Manual, CNR-ISTM, Milano (Italy), **1999**.

[21] L. Bertini, C. Gatti, unpublished results, **2003**.

[22] J. M. Ziman, *Principles of the Theory of Solids*, Cambridge University Press, Cambridge, **1972**.

[23] N. P. Blake, S. Latturner, J. D. Bryan, G. D. Stucky, H. Metiu, *J. Chem. Phys.* **2001**, *115*, 8060–8073.

[24] R. Hoffman, *A Chemist's View of Bonding in Extended Structures*, VCH, Weinheim, **1988**.

[25] Crystal structures with Zn–Zn internuclear distances shorter than 2.0 Å were all discarded in our analysis. This distance threshold, when applied to the average Zn–Zn distance in bulk Zn, corresponds to a repulsive energy whose magnitude is 4.8 times the binding energy of the crystal. The equilibrium distance in the bulk for the two different sets of six closest neighbours, equals 2.886 and 3.120 Å, respectively.

[26] The reaction which involves mixing of Zn bulk metal with the optimal 12-Zn cell structure to yield the best 13-Zn cell structure, Zn (bulk) $+ A_{12}Sb_{10} \rightarrow A_{11}BCSb_{10}$, has $\Delta E = -8$ kcal mol^{-1}. This shows that the 13-Zn cell structure is only slightly unstable with regard to disproportionation into metallic Zn and a 12-Zn structure. Furthermore, $A_{12}Sb_{10}$ is slightly unstable with regard to the formation of ZnSb and Zn metal. These reactions, when combined, corroborate the dominance of 13-Zn atom cells over Zn-12 and Zn-14 cells in the amorphous $Zn_{12.816}Sb_{10}$ phase, and they also explain the occurrence of ZnSb and Zn metal islands in experimental structure determinations.

[27] The $(BD)_{12}Sb_{10}$ structure was not considered, since it implies that the Zn–Zn distances are too short (1.87 Å).

[28] M. Tapiero, S. Tarabichi, J. G. Gies, C. Noguet, J. P. Zielinger, M. Joucla, J. Loison, M. Robino, J. Henrion, *Sol. Energy Mater.* **1985**, *12*, 257–274.

[29] There are 12 nonequivalent arrangements of $A_{10}BCDSb_{10}$ that are favoured over the coexistence of I_D and V_A in $A_{11}DSb_{10}$ when these two point defects are inserted in a pair of $A_{12}Sb_{10}$ and $A_{11}BCSb_{10}$ cells (final products in the last row against those in the first row of Table 5).

[30] For instance, if $p1$ is set to 0.05 and equal to $p2$, the Seebeck coefficients of the majority 13-Zn atom cells would rise to about 240 μV K^{-1}, while that of the minority 12-Zn atom cells would decrease to 43 μV K^{-1}.

Received: April 2, 2004
Published online: June 24, 2004

